Karlsruher Institut für Technologie

Indentation events during surface machining

- Compilation of local stress intensity factors

T. Fett, K.G. Schell, C. Bucharsky

KIT SCIENTIFIC WORKING PAPERS 163

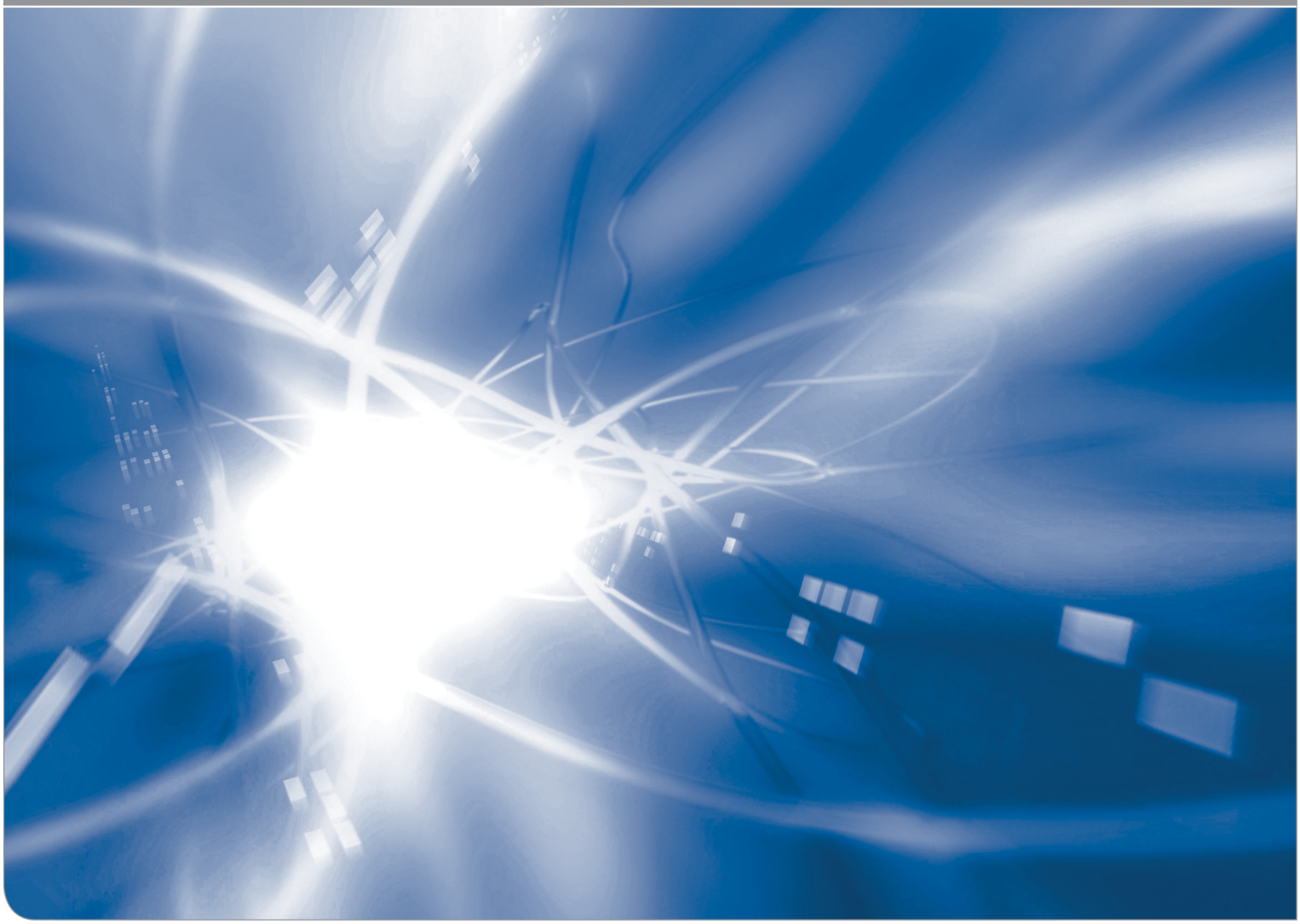

KIT – Universität des Landes Baden-Württemberg und nationales Forschungszentrum in der Helmholtz-Gemeinschaft

IAM Institute for Applied Materials

Impressum

Karlsruher Institut für Technologie (KIT)
www.kit.edu

This document is licensed under the Creative Commons Attribution – Share Alike 4.0 International License (CC BY-SA 4.0): https://creativecommons.org/licenses/by-sa/4.0/deed.en

2021

ISSN: 2194-1629

Abstract

During surface machining of glass, machining-induced surface cracks are introduced. The result of a contact between a grain of the grinding wheel and the glass surface can be described by a crack-like damage similar to the cracks obtained by hardness indentation tests.

In the present report, we study the generation of such cracks and their interaction with residual stresses in the surface region. For three different loadings (pure tension, indentation, surface stresses) we report the relevant stress intensity factors.

Contents

1. Local stress intensity factors by Newman and Raju

Cracks generated on glass surfaces during machining are responsible for reduced strength and lifetimes of mechanically loaded specimens. The same holds for artificially introduced indentation cracks. The semi-elliptical cross section of such a surface crack is shown schematically in Fig. 1a. The crack depth is *a* and the crack width is denoted as *2c*. The parametric angle along the crack front is φ and the stress acting normal on the crack plane is σ. The deepest point of the crack is generally denoted as point (A) and the intersection points at the surface as (B).

For the computation of local stress intensity factors $K(\varphi)$ under a tensile stress σ, the well established relation of Newman and Raju [1] may be used. This relation reads

$$K = \sigma Y \sqrt{a} \tag{1}$$

with the geometric function

$$Y = \frac{\sqrt{\pi}}{\mathbf{E}(1-a^2/c^2)} \underbrace{(1.13 - 0.09\tfrac{a}{c})}_{\lambda} [1 + 0.1(1-\sin\varphi)^2] \left[\left(\frac{a}{c}\right)^2 \cos^2\varphi + \sin^2\varphi \right]^{1/4} \tag{2}$$

where **E** stands for the complete elliptic integral of second kind. Figure 1b shows the geometric function $Y(\varphi)$ for several aspect ratios *a*/*c*.

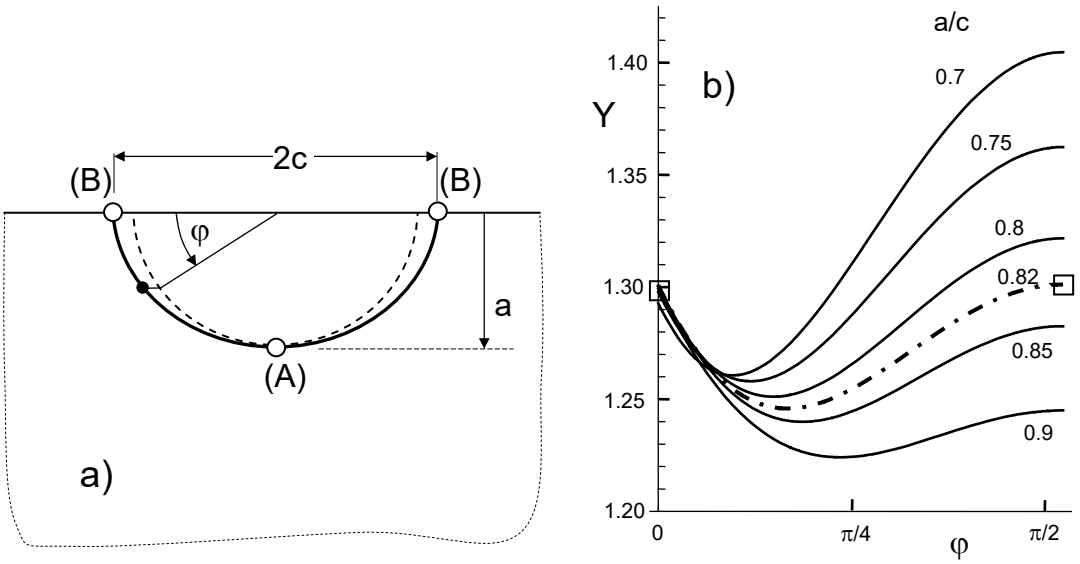

Fig. 1 a) Geometry of a semi-elliptical surface crack normal to the applied stress, b) geometric function along the crack front for several aspect ratios *a*/*c*, dash-dotted line: curve for which $Y_A = Y_B$ (represented by squares).

The geometric function at the points (B) and (A), i.e. for φ=0 and φ=π, is shown in Fig. 2a. The stress intensity factors at these points are represented in Fig. 2b. For aspect

ratios of $a/c<0.82$, the stress intensity factor is at (A) higher than at points (B). At $a/c>0.82$, the reverse applies, $K_A<K_B$.

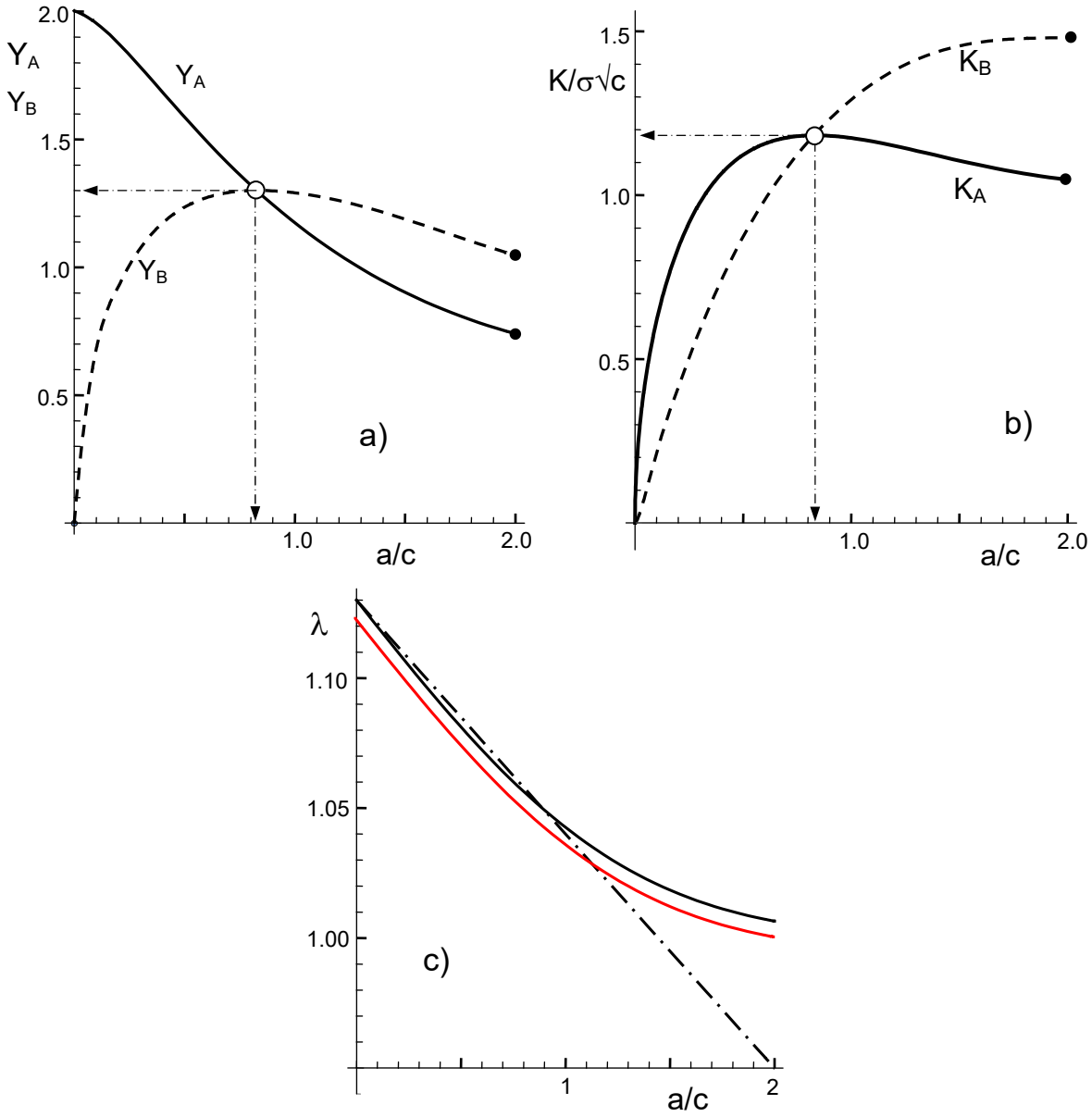

Fig. 2 Local stress intensity factors: a) geometric function at the deepest (A) and the surface points (B) of a semi-elliptical crack, b) related stress intensity factors K_A and K_B. Circles indicate $Y_A=Y_B$ and $K_A=K_B$, c) surface correction factor λ vs. aspect ratio a/c. Dash-dotted line: suggestion by Newman and Raju [1], eq.(2a), black solid curve: modified description ensuring the behavior for $a/c\to\infty$, eq.(2b), red solid curve: description including the theoretically known value for $a/c\to 0$, eq.(2c).

Two improvements of the relation eq.(2) from Newman and Raju [1] are suggested. The linear dependency of the term λ

$$\lambda = 1.13 - 0.09\frac{a}{c} \qquad (2a)$$

is shown in Fig. 2c as the dash-dotted line. This description, originally derived for $a/c \leq 1$, is not practicable for aspect ratios a/c clearly larger than $a/c=1$ since then the solution of the semi-elliptical surface crack falls below that of the embedded elliptical crack in an infinite body, $\lambda<1$, although the "free-surface effect" for the surface crack must ensure an increased stress intensity factor. Therefore, we suggest in eq.(2) a coefficient

$$\lambda = 1 + 0.13\,\mathrm{erfc}[0.692\tfrac{a}{c}] \tag{2b}$$

as plotted in Fig. 2c by the black straight line.

A second small correction is necessary since for $a/c \to 0$ the stress intensity factor at point (A) must tend to the theoretically known limit value 1.1215… (edge crack, [2,3]) instead of 1.13 obtained by Newman and Raju by FE-analysis [1]. Instead of (2b) we finally suggest

$$\lambda = 1 + 0.122\,\mathrm{erfc}[0.69\tfrac{a}{c}] \tag{2c}$$

This dependency is represented in Fig. 2c by the red curve. Consequently, the geometric function for the stress intensity factor reads

$$Y = \frac{\sqrt{\pi}}{\mathbf{E}(1-a^2/c^2)}(1+0.122\,\mathrm{erfc}[0.69\tfrac{a}{c}])[1+0.1(1-\sin\varphi)^2]\left[\left(\frac{a}{c}\right)^2\cos^2\varphi+\sin^2\varphi\right]^{1/4} \tag{2d}$$

2 Surface cracks under concentrated force

2.1 Surface crack caused during machining

During surface machining of glass machining-induced surface cracks are introduced accompanied by the generation of residual stresses [4]. Figure 3 shows a crack that has been created under a strongly localized contact between a grain of a grinding wheel and the glass surface.

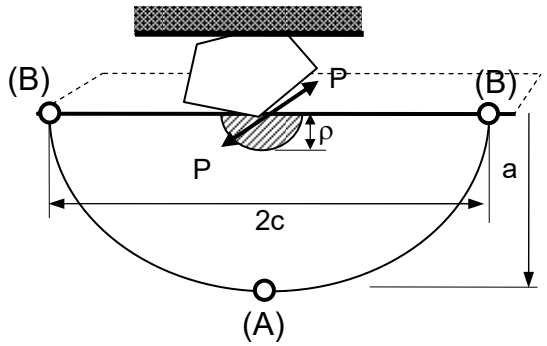

Fig. 3 Geometric data of an indentation crack: Indentation process by a single grain of the grinding wheel, resulting in a semi-elliptical surface crack of depth a and width $2c$.

The result of such a contact may be described by a crack-like damage similar to the cracks obtained by Vickers indentation tests. Beneath the contact area of indenter and glass surface, a residual stress zone of depth ρ remains even after unloading. Plastically deformed glass and material pressed between the crack flanks act as a wedge and open the crack. The result is a positive stress intensity factor $K_r>0$. If the size of the residually stressed zone is sufficiently small compared to the crack size, the stresses distributed over a cross-section of radius ρ, may be replaced by a single point force P at the crack mouth that acts perpendicularly on the crack plane.

The stress intensity factor for crack wedged by the force P, Fig. 3, is given by [5,4]

$$K_r = \chi_r \frac{P}{a^{3/2}} \tag{3}$$

where χ_r is a material-dependent proportionality coefficient. When a_0 is the crack depth from experiments in an inert environment, the relation (3) reads

$$K_{Ic} = \chi_r \frac{P}{a_0^{3/2}} \tag{4}$$

and, consequently,

$$K_r = K_{Ic}\left(\frac{a_0}{a}\right)^{3/2} \tag{5}$$

The description by eqs.(3-5) implicitly assumes a semi-circular crack contour with a constant stress intensity factor along the crack front. This may be violated especially for strongly different semi-elliptical cracks as will occur in surfaces with residual stresses.

2.2 Internal elliptical crack under a central concentrated force

Stress intensity factor solutions for embedded elliptical cracks, Fig. 4a, are known for the special case of a crack in an infinite body. Numerical results on such cracks subjected by point forces were reported by Atroshchenko [6] in Figs. 3.16 and 3.18. We evaluated these data and represent the related stress intensity factors in Figs. 4a and 4b. Curve fitting resulted in

For all a/c

$$K_B \frac{(\pi c)^{3/2}}{P} \cong 1.268(\tanh[2.105\sqrt{a/c}])^8 \tag{6}$$

or by using polynomial expressions

$$K_B \frac{(\pi c)^{3/2}}{P} \cong 1.275 \frac{2.479(a/c)^2 + 1.157(a/c)^3}{1 + 2.479(a/c)^2 + 1.157(a/c)^3} \tag{6a}$$

For $a/c \geq 0.3$

$$K_A \frac{(\pi c)^{3/2}}{P} \cong \frac{3}{a/c + (a/c)^2 + (a/c)^3} \tag{7}$$

These dependencies are entered in Figs. 4b and 4c as the curves. The difference between eqs.(6) and (6a) is less than 2% for $a/c \geq 0.3$.

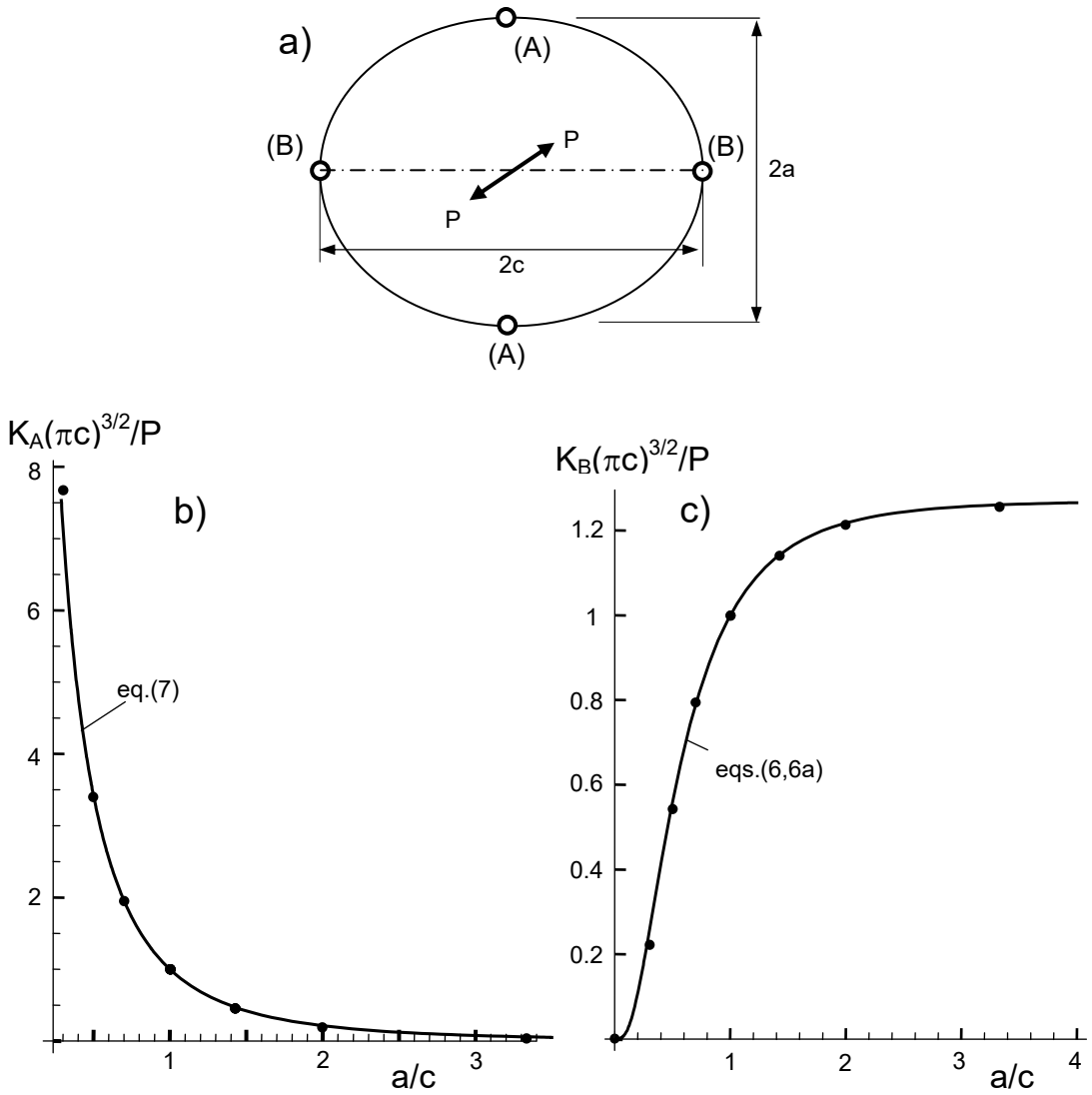

Fig. 4 Stress intensity factors for the embedded elliptical crack, a) geometry with load *P* normal on the crack plane, b) *K* at point (A), c) *K* at point (B).

2.3 Approximation of semi-elliptical cracks by internal elliptical cracks

In order to describe the semi-elliptical surface crack by half of an embedded elliptical crack needs the "free-surface correction" for point forces. To the knowledge of the authors, there are no results available in literature. Therefore, we used as an approximation the correction functions of eq.(2d).

For all *a*/*c*

$$K_B \frac{(\pi c)^{3/2}}{P} \cong 1.268(\tanh[2.105\sqrt{a/c}])^8 \lambda(\tfrac{a}{c}) \times 1.1 \tag{8}$$

$$K_B \frac{(\pi c)^{3/2}}{P} \cong 1.275 \frac{2.479(a/c)^2 + 1.157(a/c)^3}{1 + 2.479(a/c)^2 + 1.157(a/c)^3} \lambda(\tfrac{a}{c}) \times 1.1 \tag{8a}$$

with the function $\lambda(\frac{a}{c})$ given by eq.(2c).

For *a*/*c*≥0.3

$$K_A \frac{(\pi c)^{3/2}}{P} \cong \frac{3}{a/c + (a/c)^2 + (a/c)^3} \lambda(\tfrac{a}{c}) \tag{9}$$

3 Stress intensity factor for residual stresses at the surface

During machining there is not only a single crack introduced. In reality there is a high crack density available in the surface region. A detailed investigation on silica glass was carried out by Suratwala et al. [7] providing a statistical evaluation of crack size and crack densities for different surface treatments.

Since all these cracks are opened, a global compressive residual stress occurs that is indicated in Fig. 5 by a surface zone of characteristic size *b*.

In the following considerations it is assumed that the specimens were *not annealed*. Approximating the residual stresses by an erfc-shaped stress distribution below the specimen surface results in

$$\sigma_{res} \cong \sigma_0 \operatorname{erfc}\left[\frac{z}{2b}\right] \tag{10}$$

with the compressive surface stress, $\sigma_0 < 0$.

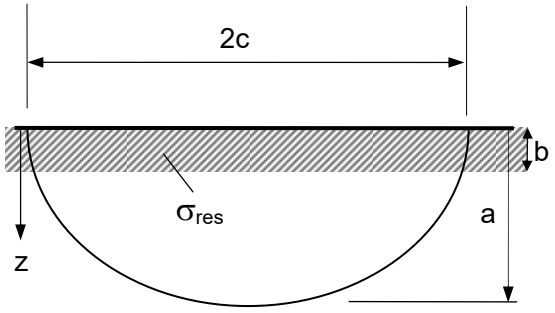

Fig. 5 Semi-elliptical crack under a continuous compressive surface stress layer σ_{res} with thickness *b* as defined by eq.(10).

The shielding stress intensity factors for semi-elliptical cracks under an erfc-shaped stress distribution, eq.(10), is according to [8]

$$K_{res,A,B,2} = \sigma_0 \sqrt{\pi\, a}\, F_{A,B} \frac{1.13 - 0.09\sqrt{\frac{a}{c}}\left\{\tanh\left[\left(\frac{a}{c}\right)^{10}\right]\right\}^{1/20}}{\sqrt{1+1.464\left(\frac{a}{c}\right)^{1.65}}} \tag{11}$$

where
$$F_A = \sum_{n=1}^{3} \frac{B_n}{1 + A_1 n \frac{a}{2b} + A_2 \left(n \frac{a}{2b}\right)^2} \tag{12a}$$

and
$$F_B = \sum_{n=1}^{3} 1.1 \sqrt{\frac{a}{c}} \frac{B_n}{1 + \left(0.1186 + 0.128\frac{a}{c} - 0.1134\frac{a^2}{c^2} + 0.0288\frac{a^3}{c^3}\right) n \frac{a}{2b}} \tag{12b}$$

The coefficients in eqs.(12a) and (12b) read:

$$A_1 = 0.43 + 0.266\left(\frac{a}{c}\right)^{0.42}, \quad A_2 = 0.266\left(\frac{a}{c}\right)^{0.42},$$

$$B_1 = -0.37664,\ B_2 = 2.7314,\ B_3 = -1.35521$$

The shielding stress intensity factors for semi-elliptical cracks in the semi-infinite body under the stresses of eq.(10), are shown in Fig. 6.

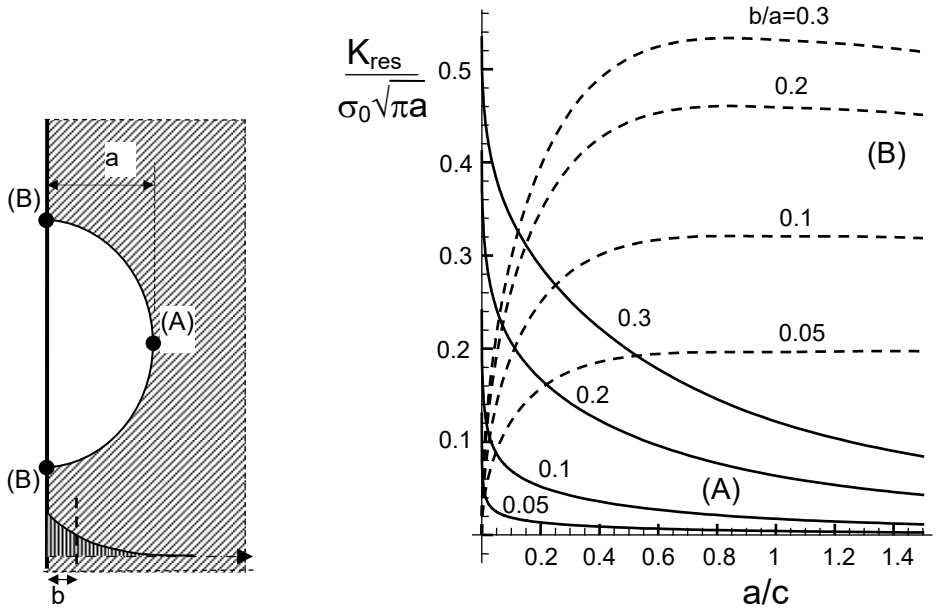

Fig. 6 Shielding stress intensity factors at the deepest point (A) and the surface points (B) of a semi-elliptical crack in a semi-infinite body [8].

4. Equilibrium crack under residual stresses

As an application of the equations given in the preceding sections, the equilibrium crack under stable crack growth conditions (i.e. for a crack with K_A=K_B) may be computed.

The total stress intensity factor during surface grinding by indentation events, K_{total}, is the sum of the wedging and the shielding stress intensity factors

$$K_{total} = K_{ind} + K_{res} \tag{13}$$

For the indentation stress intensity factor K_{ind}, here eqs.(6) and (7) are used. The initial crack size a_0 is now determined from the condition that the total stress intensity factor, K_{total}, equals the fracture toughness K_{Ic} =0.75 MPa√m, i.e.

Point (A) $$K_{ind}(A) + K_{res}(A) = K_{Ic} \tag{14a}$$

Points (B) $$K_{ind}(B) + K_{res}(B) = K_{Ic} \tag{14b}$$

The crack dimensions a and c are plotted in Fig. 7a as a function of the residual surface stress. Figure 7b represents the aspect ratio a/c of the crack. From Figs. 7a and 7b it is obvious that crack extension at the deepest point is stronger for compressive surface stresses larger than about 14 MPa. Finally, Fig. 7c shows the stress intensity factors reached after indentation in a surface, pre-stressed by the residual stress σ_0 with a thickness of b=10 µm according to eq.(10). The linearity of the curves trivially reflects the direct proportionality between K_{res} and σ_0 as expressed by eq.(11).

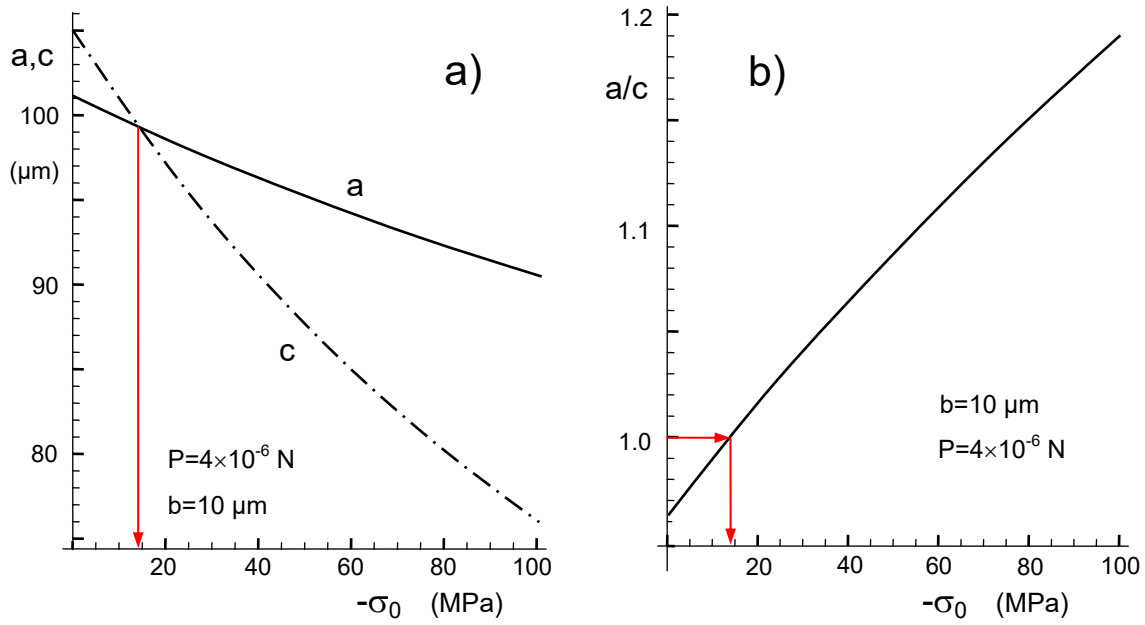

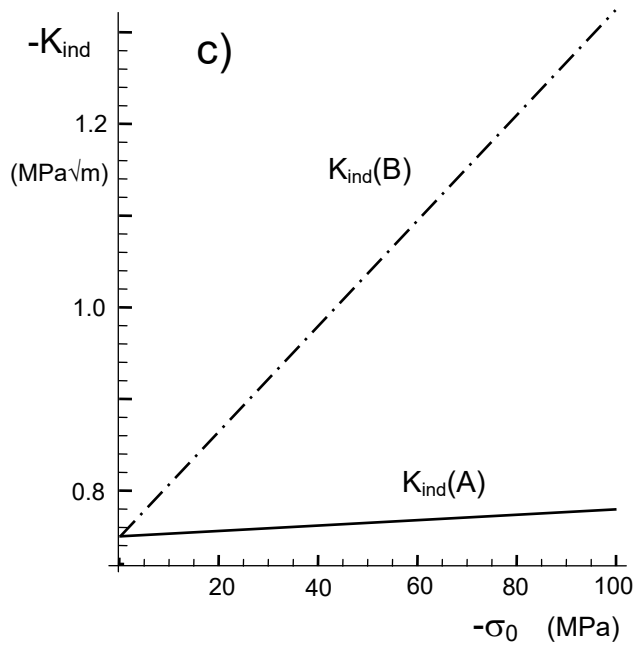

Fig. 7 Crack generation by an indentation test in a surface under residual stresses, a) crack depth a and width c as a function of the surface stress value σ_0, b) aspect ratio a/c of the semi-ellipses, c) indentation stress intensity factor K_{ind} vs. maximum residual stress at the surface (K_{Ic}=0.75 MPa√m).

Exact data depend of course on the accuracy of the "free-surface effect", underestimated here to be the same as in case of constant stresses on the crack plane [1]. Therefore, the curves in Fig. 7 can only show trends.

References

1 Newman, J.C., Raju, I.S., An empirical stress intensity factor equation for the surface crack, Engng. Fract. Mech. **15**(1981) 185-192.

2 Wigglesworth, L.A., Stress distribution in a notched plate, Mathematica **4**(1957), 76-96.

3 T. Fett, G. Rizzi, H-A. Bahr, V.B. Pham, H. Bahlke, Analytical Solutions for Stress Intensity Factor, T-Stress and Weight Function for the Edge-Cracked Half-Space, Int. J. Fract 146(2007), 189-195.

4 D.B. Marshall, A.G. Evans, B.T. Yakub, J.W. Tien, G.S. Kino, The nature of machining damage in brittle materials, Proc. R. Soc. Lond. A **385** (1983), 461-475,

5 D.B. Marshall, B.R. Lawn, J. Mater. Sci. **14** (1979), 2001.

6 E. Atroshchenko, Stress intensity factors for elliptical and semi-elliptical cracks subjected to an arbitrary mode I loading, Thesis, 2010, University of Waterloo, Ontario, Canady

7 T. Suratwala, L. Wong P. Miller, M.D. Feit, J. Menapace, R. Steele, P. Davis, D. Walmer, Sub-surface mechanical damage distributions during grinding of fused silica, J. Non-Cryst. Solids, **352**(2006), 5601-5617.

8 T. Fett, "Failure due to semi-elliptical surface cracks under arbitrary stress distributions," *Fatigue and Fracture of Engineering Materials and Structures*, **23**, S. 347-53, (2000).

KIT Scientific Working Papers
ISSN 2194-1629

www.kit.edu